PROGRESS IN COLOR, COLORANTS AND COATINGS

available online @ www.pccc.icrc.ac.ir

Progress in Color Colorants Coating 17 (2024), 263-273

Ministry of Science, Research and Technology
Institute for Color Science & Technology

Synthesis and Characterization of Nonmetal-doped TiO_2 Nanoparticles for Photocatalytic Degradation of Rhodamine B Dye

M. Karimi*, A. R. Grayeli

Physics and Accelerators Research School, Nuclear Science & Technology Research Institute (NSTRI), P.O. Box: 11365-3486, Tehran, Iran

ARTICLE INFO

Article history:
Received: 24 Oct 2023
Final Revised: 06 Jan 2024
Accepted: 08 Jan 2024
Available online: 05 Feb 2024

Keywords:
Titanium dioxide
Rhodamine B
Photocatalyst
Dye degradation
Nonmetal-doped TiO_2.

ABSTRACT

A novel series of C-, N-, and F-doped TiO_2 photocatalysts were fabricated using a simple sol-gel method, utilizing 4-(trifluoromethyl)nicotinic acid (TFNA) as a precursor for carbon, nitrogen, and fluorine doping. The resulting materials were characterized using different advanced techniques such as X-ray Diffraction (XRD), Diffuse Reflectance Spectroscopy (DRS), Raman spectroscopy, Fourier Transform Infrared Spectroscopy (FT-IR), Transmission Electron Microscopy (TEM), and Field Emission Scanning Electron Microscopy (FESEM). The synthesis approach involved the creation of nanoparticles with varying weights of TFNA, ranging from 0.3 to 1.6 wt. %, followed by calcination at 400 °C for 120 min in the presence of air. The resulting nanostructures were tested for their efficiency in degrading rhodamine B (RhB) dye under ultraviolet (UV) light irradiation. The experimental findings revealed that the 1.6 wt. % TFNA/TiO_2 composite exhibited exceptional photocatalytic activity, with approximately 87.0 % degradation efficiency towards RhB dye in aqueous solutions under UV light. This remarkable performance can be attributed to the increased lifetime of photogenerated electron-hole pairs and accelerated interfacial charge transfer rates. Prog. Color Colorants Coat. 17 (2024), 263-273© Institute for Color Science and Technology.

1. Introduction

Synthetic organic dyes, widely used in various industrial sectors such as food, paper, textiles, plastics, pharmaceuticals, cosmetics, printing, and leather, constitute a significant category of artificial carbon-based compounds. However, these substances have been identified as a primary contributor to environmental pollution, particularly in aquatic ecosystems, due to their poor biodegradability, high chemical stability, and harmful effects on living organisms. As a result, the release of artificial organic dyes into the environment has severe consequences, including carcinogenicity and toxicity, posing a significant threat to the health of aquatic life and potentially affecting human health through the food chain [1-3]. Moreover, the colored effluent from industrial processes, such as textile dyeing, contains a considerable amount of residual dye material, estimated to be around 10-15 %, which ultimately ends up in water bodies [4, 5]. These dyes possess a hazardous potential, even at minimal concentrations, owing to their toxic, carcinogenic, and mutagenic characteristics, posing a severe threat to human health and aquatic ecosystems' well-being [6]. Rhodamine B (RhB) is a widely utilized dye in various industries, including textiles, due to its excellent colorfastness properties [7]. However, it poses significant environmental and health risks due to its non-biodegradable nature and toxicity. RhB has been linked to various harmful effects, such as respiratory problems, skin and gastrointestinal irritation, eye infections, and even cancer, both in animals and humans. Its toxicity can be

*Corresponding author: * mrkarimi@aeoi.org.ir
m.karimi81@gmail.com

https://doi.org/10.30509/pccc.2024.167222.1256

attributed to its ability to cause developmental and simulative abnormalities [8]. Despite its benefits in various applications, including the production of ballpoint pens, paints, leather products, and fireworks [7], the adverse impacts of RhB necessitate proper management and disposal methods to minimize its hazards. Thus, it is crucial to treat industrial wastewater thoroughly before it is discharged to prevent the release of harmful chemicals into the environment and promote sustainable practices that prioritize eco-friendliness and human safety.

Various purification methods like biological oxidation, adsorption, and flocculation/coagulation are widely employed to treat water polluted by dyes. However, these methods generate additional pollutants (by-products) that can pose numerous challenges. As a result, industries are shifting their focus toward innovative technologies to address these issues. Recently, heterogeneous semiconductors for photocatalytic degradation under UV or visible light have gained popularity and are considered a promising approach for treating industrial wastewater using photocatalytic degradation [9, 10].

Titanium dioxide (TiO_2) has garnered significant attention among researchers due to its exceptional efficacy, excellent stability, and innocuous nature. Despite its merits, TiO_2 suffers from a substantial bandgap of 3.2 eV, which restricts its capacity to absorb visible light, thereby diminishing its photocatalytic efficiency in harnessing solar energy [11]. Researchers have explored various strategies to modify TiO_2, including co-doping with metals, nonmetals, and rare earth elements, depositing noble metals, creating semiconductor composites, and utilizing electron conductivity enhancers [12-14]. These modifications aim to improve the photocatalytic efficiency of TiO_2 by optimizing its electronic properties and augmenting its capability to harness solar energy.

There has been growing interest in doping metal oxides with nonmetallic atoms, such as carbon, nitrogen, and sulfur. Theoretical studies have revealed that the incorporation of these dopants results in significant overlap between their p-orbitals and the valence band O2p-orbitals, thus enabling efficient transfer of photo-excited charge carriers to the surface of the catalyst, which is crucial for boosting the photocatalytic activity [15]. Investigating the combined effects of multiple dopants on the optical properties, crystallinity, surface area, and activity of TiO_2 is of significant academic interest. Previous studies have shown that using two dopants can produce more pronounced improvements in visible-light absorption and photocatalytic activity than using a single dopant [16, 17]. According to studies [18-20], introducing nitrogen and fluorine impurities into TiO_2 can significantly enhance its ability to absorb visible light. The presence of doped nitrogen atoms boosts the light-absorbing properties of materials, whereas incorporating fluorine atoms creates oxygen vacancies that contribute to improved catalysis. These modifications lead to exceptional catalytic performance, making the doped TiO_2 an attractive choice for various applications.

In this research, we investigated the effectiveness of doping TiO_2 nanoparticles with nonmetallic elements to improve their photocatalytic properties. We utilized TFNA as a nitrogen, carbon, and fluorine dopant source. This approach allowed us to create modified TiO_2 materials with enhanced light-absorbing capabilities, improving their ability to initiate chemical reactions upon exposure to ultraviolet radiation. By leveraging the versatility of TFNA as a precursor, we were able to introduce multiple dopants simultaneously, leading to synergistic effects that further optimized the photocatalytic performance of the modified TiO_2. The resulting materials were thoroughly characterized using XRD, FTIR, TEM, Raman spectroscopy, FESEM, and DRS techniques. We assessed the photocatalytic performance of the dopant-modified TiO_2 by examining its capability to degrade RhB under UV illumination.

2. Experimental

2.1. Materials

In this work, titanium tetra isopropoxide (TTIP) and 4-(Trifluoromethyl) nicotinic acid (4-TFNA) (98 wt. %) (Figure 1) were purchased from Sigma-Aldrich. Acetic acid, hydrochloric acid, sodium hydroxide, and ethanol were purchased from Merck Company. The synthetic dye used for studying the photocatalytic activity was Rhodamine B (RhB), supplied by Sigma Aldrich. Deionized water was used during the experiments. All substances and solvents have been used without further purification.

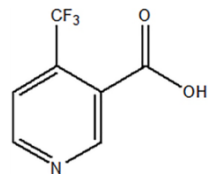

Figure 1: Chemical structure of 4-TFNA.

2.2. Synthesis of TFNA/TiO_2 composites

To synthesize nanoscale photocatalysts featuring nonmetal atoms, 4-TFNA served as the precursor. A protocol was established for its preparation, which entailed the following steps: Initially, a mixture of 20 mL of ethanol and 9 mL of glacial acetic acid was prepared in a flask and stirred for approximately 15 minutes in an ice bath under a nitrogen atmosphere. Subsequently, 4.7 mL of TTIP was continuously stirred into the mixture. This mixture was then stirred for around 30 min in an ice bath under a nitrogen atmosphere. Afterwards, deionized water containing varying concentrations (0, 0.3, 0.6, or 1.6 wt. %) of TFNA was slowly introduced into the mixture via dropwise addition, accompanied by rigorous stirring for 60 minutes. The solution was then subjected to ultrasonic treatment for an additional hour. The resulting solution was kept in darkness overnight to allow nucleation and subsequently gelled at 70 °C for 12 hours. Finally, the gel was dried at 110 °C and then exposed to heat treatment at 400 °C for 120 minutes in the presence of air, yielding crystalline nano photocatalysts. Pure TiO_2 was obtained by eliminating TFNA using an identical method.

2.3. Instrumentation

X-ray diffraction analysis was conducted utilizing an EQUINOX3000 X-ray diffractometer manufactured by Intel Company in France, equipped with Cu Kα radiation (λ = 1.541874 nm). The XRD scanning process occurred at a rate of 0.1° per minute, covering an angular range of $3° < 2\theta < 85°$. The current and acceleration voltages were set at 30 mA and 40 kV, respectively.

Raman analysis was performed using a Thermo Scientific DXR Raman microscope equipped with a 532 nm laser source. Additionally, FT-IR spectroscopy was carried out using a Bruker VERTEX70 instrument with KBr pellets. The absorption spectra of Rhodamine B (RhB) were recorded over 200 to 600 nm using a PerkinElmer Lambda 45 UV-Vis spectrophotometer.

TEM imaging of the samples was achieved through a Zeiss EM10C microscope operating at an accelerating voltage of 100 kV. Furthermore, a MIRA3TESCAN-XMU FE-SEM was employed to investigate the morphology of the prepared materials. Before conducting the FE-SEM measurement, a thin layer of gold was deposited onto the sample surface to prevent charge buildup.

2.4. Experimental procedure

The efficiency of the nano photocatalysts was evaluated by measuring their ability to degrade rhodamine B in an aqueous solution under UV light (Scheme 1). To conduct the photocatalytic experiments, 30 mg of the nano photocatalyst was introduced into a 100 mL solution containing ten ppm of rhodamine B in a glass vessel with a diameter of 8.5 cm. The mixture was then stirred for approximately 60 minutes in the dark to allow for equilibrium between the adsorption processes of the photocatalyst and the analyte. Afterwards, the quantity of dye adsorbed on the photocatalyst surface was measured every 20 minutes for 60 minutes, utilizing a UV-Vis spectrometer.

Next, the photocatalytic reaction was initiated by exposing the suspension to UV irradiation produced by a HAICHAO-F8T5 GL lamp (emitting at 254 nm with an intensity of 8 W) while maintaining constant agitation (500 rpm). The distance between the light source and the reaction vessel was around 24 centimetres. Moreover, a controlled trial was performed without introducing any photocatalyst for comparison. Throughout the reaction, 5 mL portions of the suspension were taken out at 10-minute intervals for UV-Vis analysis. The samples were centrifugated at 8000 rpm for 12 minutes to separate the photocatalyst from the remaining solution. Next, the amount of remaining rhodamine B was determined by measuring its absorbance at its peak wavelength (562 nm) using a UV-Vis spectrophotometer.

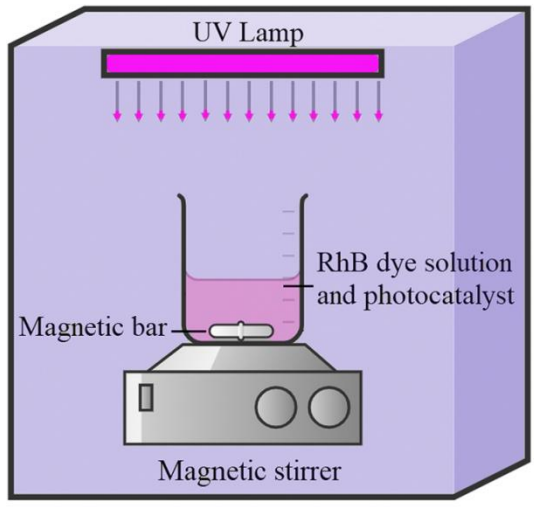

Scheme 1: Schematic of the photocatalytic experimental setup.

3. Results and Discussion

3.1. Characterization of photocatalyst

3.1.1. XRD measurements

The crystalline nature of the synthesized TiO_2 and nonmetal-doped TiO_2 has been thoroughly examined using XRD analysis, and the resulting patterns are depicted in Figure 2. In the case of undoped TiO_2 NPs, the diffraction peaks observed can be readily attributed to the tetragonal anatase structure of TiO_2, exhibiting excellent correspondence with the reference pattern recorded in the Joint Committee on Powder Diffraction Standards (JCPDS) under the entry code No. 00-001-0562. Introducing nonmetals into the TiO_2 matrix does not give rise to new diffraction peaks, indicating that the crystal structure remains unaltered. This observation confirmed the phase purity of the nonmetal-doped TiO_2 NPs, implying that the incorporation of TFNA does not change the anatase phase.

3.1.2. Raman spectra

Raman spectroscopy is a valuable tool for analyzing metal oxides, providing information on their chemical composition and structural properties without damaging the sample. The Raman spectra of the synthesized compounds, displayed in Figure 3, reveal a rich landscape of vibrational modes, providing a fingerprint of the underlying chemical species. Of particular note, the spectrum of pure anatase exhibits well-defined bands at 144, 394, 514, and 636 cm^{-1}, which have been previously assigned to various vibrational modes, including Eg, B1g, A1g or B1g, and Eg vibrations [21]. These characteristic peaks are a hallmark of the anatase crystal structure and provide clear evidence for its presence within the synthesized TFNA/TiO_2 composites. Remarkably, a thorough examination of the Raman spectra reveals that the intensity and position of these anatase-specific bands remain largely unaffected by

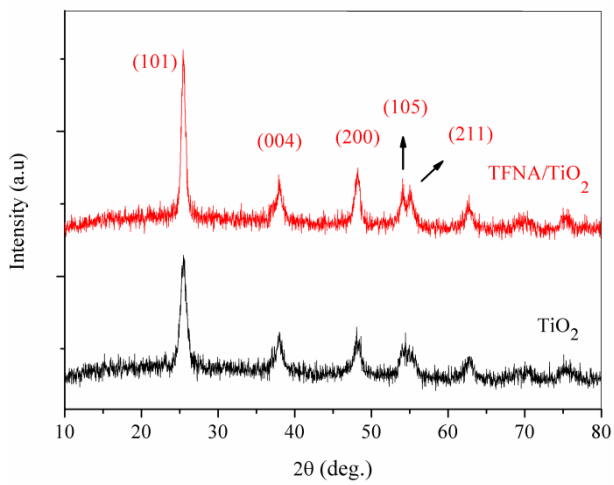

Figure 2: XRD diffractograms of TiO_2 and TFNA/TiO_2.

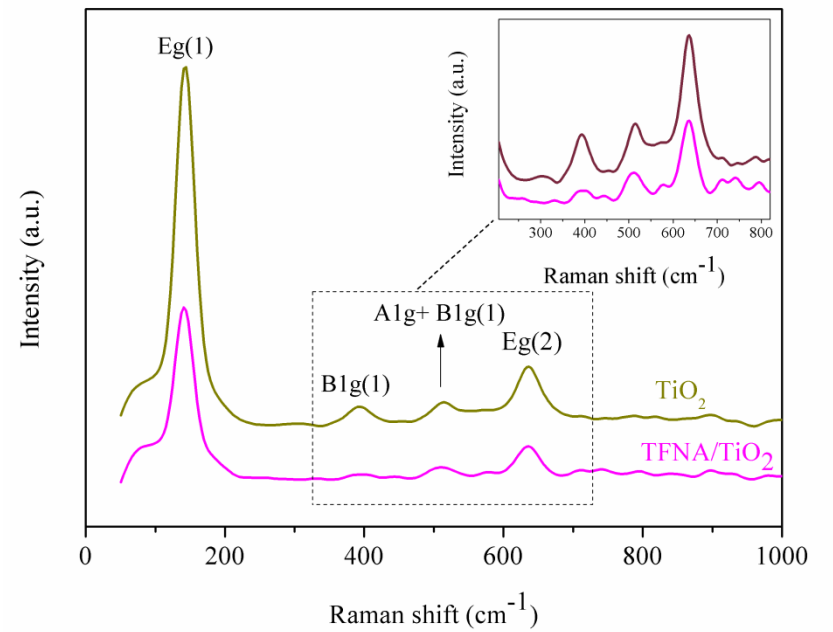

Figure 3: Raman spectra of prepared materials.

the incorporation of TFNA. This observation attests to the stability and integrity of the anatase phase in the face of nonmetal doping, suggesting that the introduced defects do not significantly alter the crystal lattice. Consequently, the Raman results support the successful synthesis of TFNA/TiO_2 nanocomposites, wherein the anatase framework is preserved while benefiting from the unique properties of the incorporated nonmetals.

3.1.3. FESEM and TEM images

The morphological characteristics of the synthesized materials were investigated using FESEM [22]. Figures 4a and b show the FESEM images of the TiO_2 and TFNA/TiO_2 samples, respectively, which reveal a spherical shape and partial aggregation for both photocatalysts. Notably, introducing TFNA into the TiO_2 framework did not alter the morphology of the TiO_2 nanoparticles. The FESEM images revealed that the particle sizes of TFNA/TiO_2 ranged from 20 to 30 nm, corroborating the findings from the XRD analysis. TEM was utilized to examine the particle size and morphology of the prepared samples. TEM imaging allows for the visualization of the internal structure of particles and provides precise measurements of their size and shape [14, 23, 24]. The TEM images, shown in Figures 4c and d, display spherical shapes for TiO_2 and TFNA/TiO_2 nanoparticles, with some aggregation. The diameter of the TFNA/TiO_2 nanoparticles was determined to be between 20-30 nm from the micrographs, which aligns with the findings from SEM. Additionally, elemental mapping (Figure 5a-f) demonstrated a uniform F, C, and N distribution throughout the anatase nanoparticles.

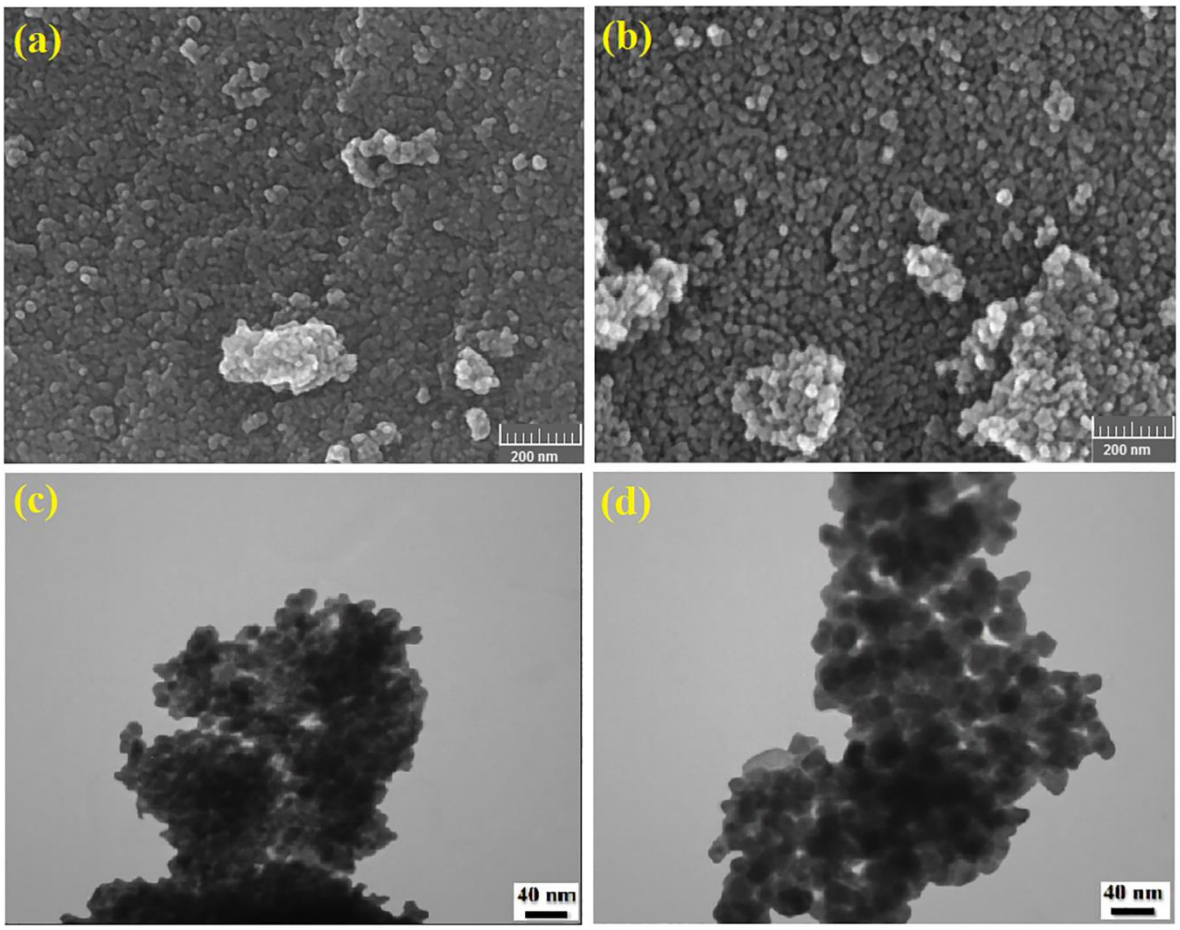

Figure 4: FESEM micrographs a) pure TiO_2, b) 1.6 wt. % TFNA/TiO_2, and TEM image of c) pure TiO_2, and d) 1.6 wt. % TFNA/TiO_2.

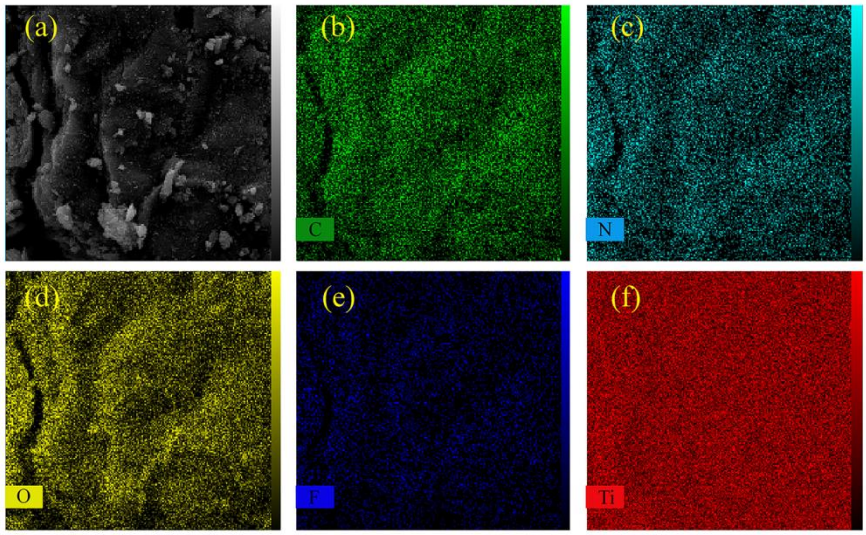

Figure 5: a) SEM image and b-f) elemental mapping of 1.6 wt. % TFNA/TiO_2 photocatalyst.

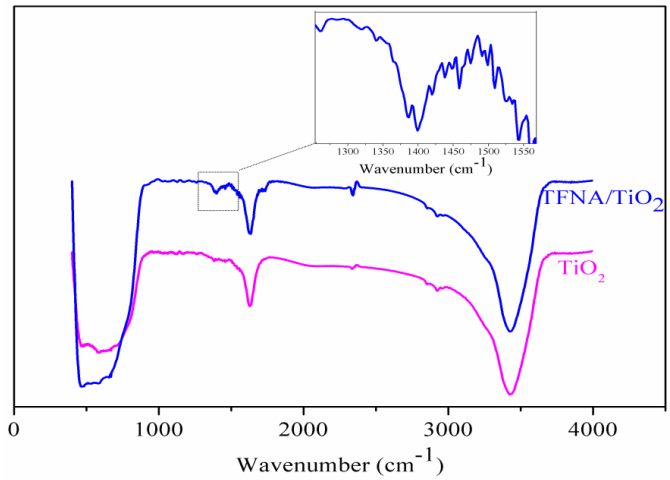

Figure 6: FTIR spectra of prepared materials.

3.1.4. FTIR spectroscopy

The FT-IR spectra of TiO_2 samples, both undoped and tridoped, exhibit distinctive features that provide insight into their chemical composition (Figure 6). Two prominent absorption bands, at 3432 cm^{-1} [25] and 1631 cm^{-1}, can be attributed to the stretching and bending vibrations of hydroxyl groups (O-H), indicating the presence of moisture in the sample. The 400 to 800 cm^{-1} signals are likely associated with the stretching vibrations of Ti-O-Ti or Ti-O-C bonds in the doped TiO_2 and TiO_2-based hybrid [12]. Notably, a peak at 1386 cm^{-1}, corresponding to C-O stretching in carboxylic acid, is observed only in the TFNA/TiO_2 spectrum, further supporting the notion of dopant incorporation.

3.1.5. Diffuse reflectance spectroscopy

The UV−Vis DRS of TiO_2 and nonmetal-doped TiO_2 is depicted in Figure 7. The pristine TiO_2 nanoparticles displayed a band gap of approximately 3.26 eV. In contrast, the TFNA/TiO_2 nanocrystals revealed band gaps of around 3.21, 3.08, and 3.06 eV, corresponding to 0.3, 0.6, and 1.6 wt. % TFNA loading, respectively. Notably, the 1.6 wt. % TFNA/TiO_2 nanocrystals exhibited a reduced band gap and a blue shift of nearly 0.2 eV relative to the pristine TiO_2 nanoparticles. These findings suggest that the 1.6 wt. % TFNA/TiO_2 nanocrystals possess enhanced photocatalytic activity under UV irradiation.

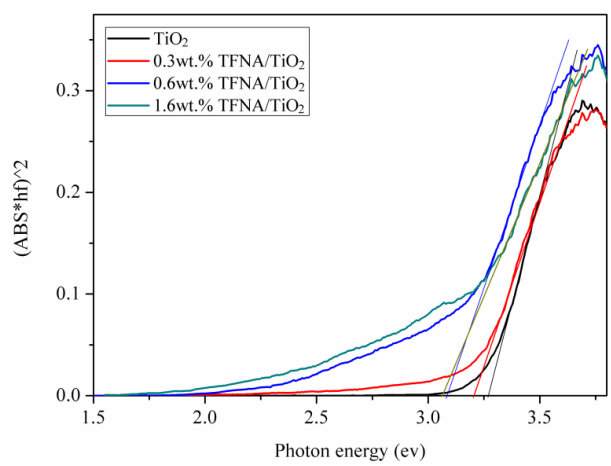

Figure 7: Tauc plots of TiO_2 and nonmetal-doped TiO_2.

The mechanism behind the enhanced photocatalytic activity of C, N, and F co-doped TiO_2 can be attributed to several factors, including band gap narrowing, valence band energy level modifications, and oxygen vacancies. The overlapping of C2p, N2p, and F2p hybrid orbitals with the O2p orbital in anatase TiO_2 leads to a significant decrease in the band gap. Additionally, substituting oxygen sites with carbon, nitrogen, and fluorine atoms raises the energy level of the valence band. Finally, the presence of oxygen-deficient sites in the grain boundaries of TiO_2, which can be stabilized by co-doping with C, N, and F, helps to prevent re-oxidation and maintain the photocatalytic efficiency of materials [12].

3.2. Photocatalytic degradation

The efficiency of the nanoscale photocatalysts in degrading organic pollutants was evaluated by examining their ability to degrade RhB under UV irradiation. The extent of photocatalytic degradation was quantified using the following equation (Eq. 1):

$$dye\ degradation\ (\%) = \left(\frac{A_0 - A_i}{A_0}\right) \times 100 \qquad (1)$$

A_o and A_i are the RhB initial absorbance and absorbance after photocatalytic decomposition, respectively.

3.2.1. Effect of TFNA content

The degradation rate of Rhodamine B (RhB) was investigated using various photocatalysts, including pure TiO_2 and tri-doped titanium oxide (TFNA/TiO_2), and the results are displayed in Figure 8. It was found that the adsorption of the dye onto the photocatalyst surface was negligible in the absence of light. Additionally, the degradation of RhB in the absence of a photocatalyst was examined, revealing a low degradation rate of approximately 20 % after 100 minutes. This suggests that direct photolysis under natural sunlight is inadequate for degrading RhB. Also, the photocatalytic activity of pure TiO_2 and TFNA/TiO_2 for RhB degradation was compared. The findings revealed that the degradation rate of RhB increased significantly for all TFNA/TiO_2 catalysts, indicating that doping enhances the photocatalytic performance of TiO_2 under UV light. Specifically, the degradation rate improved from 66 to 86 % as the amount of TFNA increased from 0.3 to 1.6 wt. %. This improvement in photocatalytic performance can be attributed to the efficient separation of charge carriers and reduced band gap in the TiO_2 lattice due to nonmetal doping.

3.2.2. Effect of pH

The pH of the solution significantly impacts the decontamination process, as it influences the surface characteristics of the catalysts, the properties of the organic dyes, and the reaction kinetics. Thus, the Effect of initial solution pH levels (ranging from 2.0 to 8.0) on the decomposition of rhodamine B when exposed to UV light was assessed. According to Figure 9, the efficiency of the photocatalyst showed an upward trend as the initial pH level was raised from 2.0 to 4.0 and 5.0, reaching performances from 73.8 to 83.2 % and 87.0 %, respectively. However, beyond these pH values,

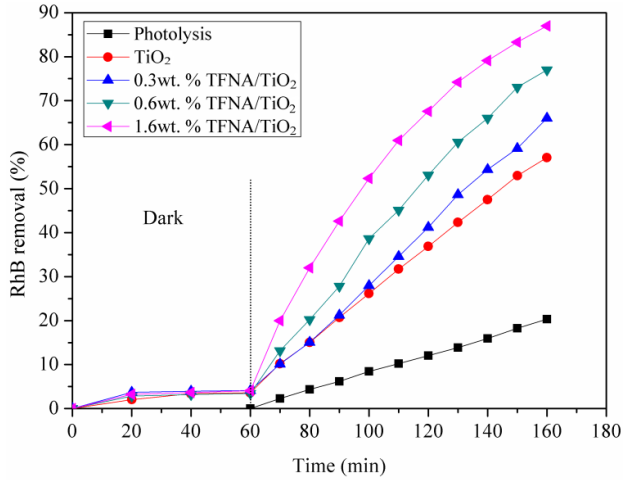

Figure 8: Photodegradation of RhB under UV irradiation over TiO_2 and (0.3-1.6 wt. % TFNA/TiO_2) photocatalyst.

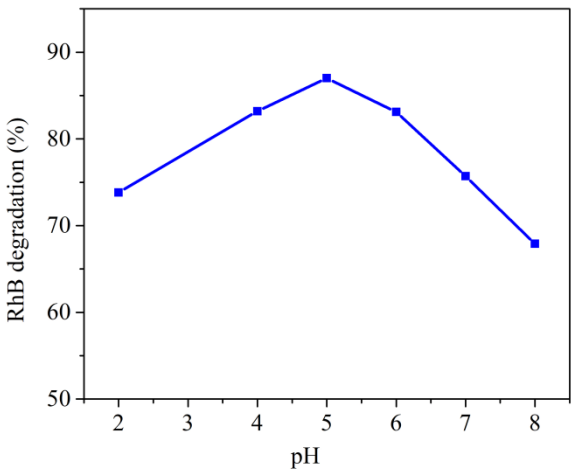

Figure 9: The Effect of pH on photodegradation of RhB under UV irradiation using 1.6 wt. % TFNA/TiO_2 photocatalyst at a time of 100 min.

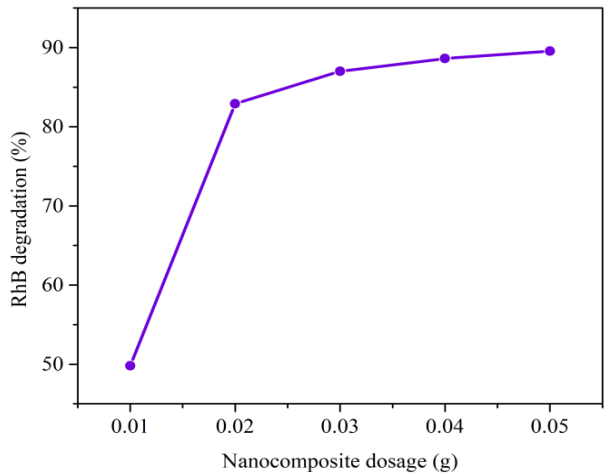

Figure 10: The Effect of nanocomposite dosage on photodegradation of RhB under UV irradiation using 1.6 wt. % TFNA/TiO_2 photocatalyst at a time of 100 min and pH 5.

the performance began to decline, dropping to 83.1, 75.7, and 67.9 % at 6.0, 7.0, and 8.0, respectively. The TiO_2/TFNA nanocomposite exhibited a pH_{ZPC} of approximately 5.5. Consequently, the surface of the photocatalyst carries a negative charge at pH values above 5.5, whereas it becomes positively charged at lower pH values. Notably, the acid dissociation constant (pKa) of RhB is 3.1 [26], implying that the dye molecule is positively charged at pH values below 3.1 and negatively charged at pH above 3.1. The degradation efficiency of the photocatalytic system is diminished under highly acidic conditions, as illustrated in Figure 9, due to the positive charging of both the catalyst and dye molecule surfaces. These results in repulsion between the dye molecules and the catalyst, hindering their approach and subsequent degradation. Raising the initial pH from 2.0 to 5.0 enhances the efficiency of the photocatalyst because the charges on the catalyst surface and rhodamine B are opposite, resulting in a strong, attractive force between them. Conversely, the decolourization efficiency decreases at pH values above 5.0 due to the intense repulsion between the TFNA/TiO_2 surface and dye molecules. Therefore, the pH value of 5.0 was selected as an optimum value for the photocatalytic degradation of rhodamine B.

3.2.3. Effect of TFNA/TiO_2 nanocomposite dosage

The photocatalytic activity of TFNA/TiO_2 was investigated using various catalyst loadings (0.01-0.05 g) to determine the optimal amount for decolorization (Figure 10). The results showed an improvement in degradation rate from 49.8 to 87.0 % as the catalyst loading increased from 0.01 to 0.03 g. This enhancement can be attributed to the increased adsorption capacity and generation rate of reactive species on the surface of the nanocomposite due to the higher TFNA/TiO_2 content and surface area. However, no significant improvements in degradation efficiency were observed at catalyst loadings above 0.03 g, likely due to the aggregation of the catalyst, which resulted in a constant number of active sites. Consequently, a dosage of 0.03 g was determined to be the optimal amount of TFNA/TiO_2 for efficient photocatalytic decolorization.

3.3. Comparison of adsorption, photolysis, and photocatalysis of RhB

The degradation of a molecule through exposure to specific wavelengths of light, known as photolysis, is a natural process that occurs independently of any external influences. Adsorption, another natural phenomenon, also occurs spontaneously and can simultaneously take place alongside photocatalysis. To accurately assess the effectiveness of photocatalysis, it is essential to consider the potential impact of these concurrent natural processes, which were studied before the development of photocatalytic methods [27]. Numerous studies have employed comparable methodologies to investigate the same phenomenon in this area of research [27, 28]. The results are shown in Figure 11. The RhB dye with an initial concentration of 10 mgL^{-1} exhibited prominent absorption peaks at 562 nm. Before photocatalysis, an adsorption step of 60 minutes was employed at dark,

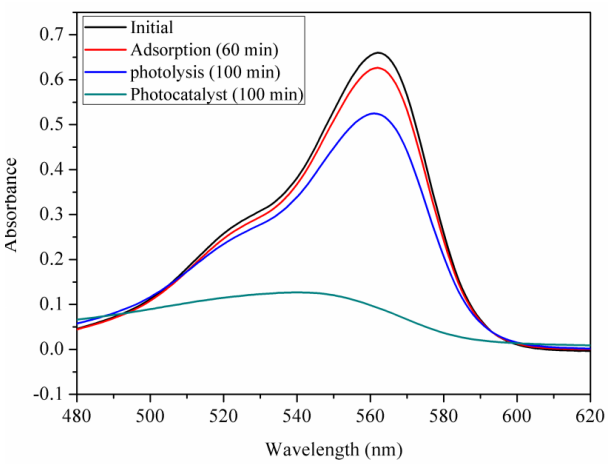

Figure 11: UV-Vis absorption spectra of RhB at different conditions.

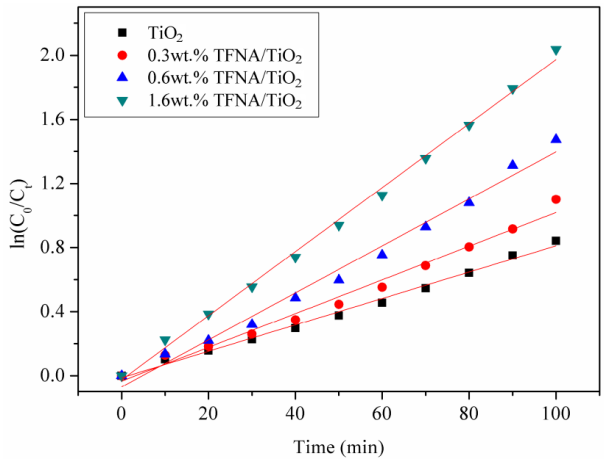

Figure 12: First-order kinetic model adjustment [ln (C_0/C) vs radiation time(min)] for RhB degradation with different photocatalysts.

resulting in a mere 4 % removal of RhB, indicative of a limited adsorption capacity of TFNA/TiO_2 towards the dye. Without a photocatalyst, photolysis under UV light gradually degraded RhB, with a moderate removal rate of approximately 20 % after 100 minutes. However, upon incorporating TFNA/TiO_2 as a photocatalyst, a drastic decrease in the UV-Vis spectrum peak intensity was observed, signifying enhanced degradation of RhB. Notably, the dye removal degree increased to 86 % following 100 minutes of irradiation, highlighting the efficacy of TFNA/TiO_2 in degrading RhB under UV light.

The findings conclusively demonstrate the photocatalytic nature of the chemical reaction, with the doped-TiO_2 particles being the primary activation source. Upon absorbing UV radiation, these particles generate highly reactive species, including hydroxyl radicals (HO•), responsible for degrading the RhB dye in solution [29, 30].

3.4. Kinetic study

The kinetic analysis of the photodegradation process was conducted on all samples, and the resulting data are presented in Figure 12. The study revealed that the degradation of RhB dye followed pseudo-first-order kinetics, which can be mathematically represented by the equation 2.

$$\ln\left(\frac{C_o}{C_t}\right) = K_{app}t \qquad (2)$$

Here, C_o and C_t represent the concentration of RhB at time zero and time t, respectively, while K_{app} is the apparent pseudo-first-order rate constant. The linear correlation between ln (C_o/C_t) and irradiation time confirmed that the photodegradation process conformed to pseudo-first-order kinetics. The K_{app} was determined by analyzing the slope of the plot of ln (C_o/C_t) against time.

The experimental data showed that the value of K_{app} increased with increasing content of TFNA in TFNA/TiO_2 photocatalysts. Specifically, the estimated K_{app} were 0.008, 0.010, 0.015, and 0.020 min^{-1} for pure TiO_2, and 0.3, 0.6, and 1.6 wt. % TFNA in TFNA/TiO_2 photocatalysts, respectively.

These findings suggest that the enhanced degradation efficiency of the 1.6 wt. % TFNA/TiO_2 photocatalyst can be attributed to improved charge carrier separation and transport properties. Including C, N, and F impurities in the photocatalyst promotes effective electron transfer and hinders recombination reactions, producing exceptional photocatalytic performance. Consequently, the 1.6 wt. % TFNA/TiO_2 photocatalyst demonstrated the highest degradation efficiency among all the samples studied.

3.5. Energy Level Structure

Theoretical calculations based on Mulliken electronegativity theory have been employed to determine the energy levels of the valence band (VB) and conduction band (CB) of both pure TiO_2 and doped TiO_2 nanomaterials (Eqs. 3 and 4) [31]:

$$E_{VB}=X-E^e+0.5E_g \qquad (3)$$

$$E_{CB}=E_{VB}-E_g \qquad (4)$$

Specifically, the VB potential (E_{VB}), electron energy (E^e=4.5 eV), CB potential (E_{CB}), band gap width (E_g), and the absolute electronegativity of TiO_2 (X) were used to estimate the energies of the bands. According to previous research, the absolute electronegativity of TiO_2 has been reported to be 5.81 eV [31]. Using the given values and formulae, the VB and CB energies for pure TiO_2 and doped-TiO_2 nanomaterials were computed and compiled in Table 1. Notably, the results show that 1.6 wt. % TFNA/TiO_2 nanomaterials exhibit a lower CB and VB position than other TFNA/TiO_2 samples and pure TiO_2. This suggests that the electrons can move more quickly toward the surface, enhancing the photocatalytic efficiency in degrading RhB dye under UV light irradiation.

Table 1: The calculated energy level of VB and CB of nanomaterials

Nanomaterials	Band gap (E_g, eV)	E_{VB} (eV)	E_{CB} (eV)
Pure TiO_2	3.26	2.94	-0.32
0.3 wt. % TFNA/TiO_2	3.21	2.92	-0.29
0.6 wt. % TFNA/TiO_2	3.08	2.85	-0.23
1.6 wt. % TFNA/TiO_2	3.06	2.84	-0.22

3.6. Proposed mechanism

The mechanism pathway for the photodegradation of RhB by TFNA/TiO_2 photocatalyst upon ultraviolet (UV) light activation is depicted in scheme 2. When exposed to UV radiation, electrons residing in the valence band of TiO_2 are excited to the conduction band while generating an equal number of photoinduced holes in the valence band. These holes can effectively oxidize the RhB dye molecules that are adsorbed on the catalyst's surface via a face-to-face interaction. Additionally, dissolved oxygen (O_2) in the surrounding aqueous medium can efficiently capture the electrons at the catalyst's surface, forming superoxide radical anions (O_2•$^-$). Alongside the holes, superoxide radical anions, and hydroxyl radicals (OH•) also contribute to the breakdown of RhB dye into environmentally friendly intermediate products through reactions involving these reactive species.

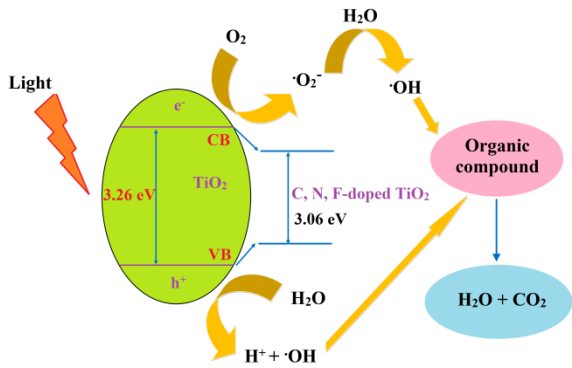

Scheme 2: Proposed mechanism pathway for RhB degradation with pure TiO_2 and doped TiO_2 nanomaterials.

4. Conclusion

In conclusion, the present study reports the successful synthesis and characterization of nonmetal-doped TiO_2 nanoparticles using TFNA as a novel precursor for the first time. The results demonstrate that TFNA is a versatile and efficient precursor for doping TiO_2 with multiple nonmetallic elements, including nitrogen, carbon, and fluorine. The findings of this study suggest that 1.6 wt. % TFNA/TiO_2 is an efficient catalyst for the decontamination of RhB and other similarly low biodegradable pollutants, as well as real industrial wastewater, when subjected to UV irradiation.

5. References

1. Ahmad M, Qureshi MT, Rehman W, Alotaibi NH, Gul A, Abdel Hameed RS et al. Enhanced photocatalytic degradation of RhB dye from aqueous solution by biogenic catalyst Ag@ZnO. J Alloys Compd. 2022; 895: 162636. https://doi.org/10.1016/j.jallcom.2021.162636.
2. Rafiq A, Ikram M, Ali S, Niaz F, Khan M, Khan Q, et al. Photocatalytic degradation of dyes using semiconductor photocatalysts to clean industrial water pollution. J Ind Eng Chem. 2021; 97(25): 111-128. https://doi.org/10.1016/j.jiec.2021.02.017.
3. Noukelag SK, Razanamahandry LC, Ntwampe SKO, Arendse CJ, Maaza M. Industrial dye removal using bio-synthesized Ag-doped ZnO nanoparticles. Environ Nanotechnol Monit Manag. 2021; 16: 100463. https://doi.org/10.1016/j.enmm.2021.100463.

4. Panchal D, Sharma A, Pal S. Novel photocatalytic techniques for organic dye degradation in water In Photocatalytic Degradation of Dyes; Elsevier: Amsterdam, The Netherlands, 2021; pp. 1-22.
5. Shreema K, Mathammal R, Kalaiselvi V, Vijayakumar S, Selvakumar K, Senthil K, Green synthesis of silver doped zinc oxide nanoparticles using fresh leaf extract Morinda citrifoliaand its antioxidant potential. Mater Today: Proc. 2021; 47: 2126-2131. https://doi.org/10.1016/j.matpr.2021.04.627.
6. Abutalib MM, Rajeh A. Influence of ZnO/Ag nanoparticles doping on the structural, thermal, optical and electrical properties of PAM/PEO composite. Phys B: Condens. 2020; 578(1): 411796. https://doi.org/10.1016/j.physb.2019.411796.
7. Panchal P, Paul DR, Sharma A, Hooda D, Yadav R, Meena P, et al. Phytoextract mediated ZnO/MgO nanocomposites for photocatalytic and antibacterial activities. J Photochem Photobiol A: Chem. 2019; 385: 112049. https://doi.org/10.1016/j.jphotochem.2019. 112049.
8. Xie Y, Liu T, Chu Z, Jin W. Recent advances in electrochemical enzymatic biosensors based on regular nanostructured materials. J Electroanal Chem. 2021; 893(15): 115328. https://doi.org/10.1016/j.jelechem.2021.115328.
9. Khalid NR, Mazia U, Tahir MB, Niaz NA, Javid MA. Photocatalytic degradation of RhB from an aqueous solution using Ag_3PO_4/N-TiO_2 heterostructure. J Mol Liq. 2020; 313(1): 113522. https://doi.org/10.1016/j.molliq.2020.113522.
10. Rotami M, Hamadanian M, Rahimi-Nasrabadi M, Ganjali MR. Sol-gel preparation of metal and nonmetal-codoped TiO_2–graphene nanophotocatalyst for photodegradation of MO under UV and visible-light irradiation. Ionics. 2019; 25: 1869-1878. https://doi. org/10.1007/s11581-019-02861-5.
11. Ton NNT, Dao ATN, Kato K, Ikenaga T, Trinh DX, Taniike T. One-pot synthesis of TiO_2/graphene nanocomposites for excellent visible light photocatalysis based on chemical exfoliation method. Carbon. 2018; 133: 109-117. https://doi.org/10.1016/j.carbon.2018.03.025.
12. Nenavathu BP, Kandula S, Verma S. Visible-light-driven photocatalytic degradation of safranin-T dye using functionalized graphene oxide nanosheet (FGS)/ZnO nanocomposites. RSC Adv. 2018; 8: 19659-19667. https://doi.org/10.1039/C8RA02237B.
13. Yang X, Cao C, Erickson L, Hohn K, Maghirang R, Klabunde K, Photo-catalytic degradation of Rhodamine B on C-, S-, N-, and Fe-doped TiO_2 under visible-light irradiation. Appl Catal B. 2009; 91(3-4): 657-662. https://doi.org/10.1016/j.apcatb.2009.07.006
14. Yang X, Cao C, Hohn K, Erickson L, Maghirang R, Klabunde K. Highly visible-light active C- and V-doped TiO_2 for degradation of acetaldehyde. J Catal. 2007; 252(2): 296-302. https://doi.org/10.1016/j.jcat.2007.09.014.
15. Yang X, Cao C, Erickson L, Hohn K, Maghirang R, Klabunde K. Synthesis of visible-light-active TiO_2-based photocatalysts by carbon and nitrogen doping. J Catal. 2008; 260(1): 128-133. https://doi.org/10.1016/j.jcat.2008.09.016.
16. Lee J S, You KH, Park C B. Highly photoactive, low bandgap TiO_2 nanoparticles wrapped by graphene. Adv Mater. 2012; 24(8): 1084-1088. https://doi.org/10.1002/adma.201104110.
17. Jiang L, Gao X, Chen S, Ashok J, Kawi S. Oxygen-Deficient WO_3/TiO_2/CC Nanorod Arrays for Visible-Light Photocatalytic Degradation of Methylene Blue. Catalysts. 2021; 11(11): 1349. https://doi.org/10.3390/catal11111349..

How to cite this article:
Karimi M, Grayeli AR. Synthesis and Characterization of Nonmetal-doped TiO_2 Nanoparticles for Photocatalytic Degradation of Rhodamine B Dye. Prog Color Colorants Coat. 2024;17(3):263-273. https://doi.org/10.30509/pccc.2024.167222.1256.